Environmental Earth Sciences (2019) 78:341
https://doi.org/10.1007/s12665-019-8342-9

ORIGINAL ARTICLE

Cooperative inversion of magnetotelluric and seismic data on Shurab diapirs in Central Iran

M. Moradi[1] · B. Oskooi[1,2] · P. Pushkarev[3] · M. Smirnov[2] · H. Esmaeili Oghaz[4]

Received: 22 July 2018 / Accepted: 21 May 2019 / Published online: 31 May 2019

Abstract

Using diapirs as liquid or gas storage structures has increased because salt formations are considered to be extremely impermeable and non-reactive. The process of delineating the diapirs' structures ends in lots of challenges due to their geological complexity. Therefore, the integration of different geophysical methods seems to be necessary to cover different physical characteristics of the diapirs. Shurab diapirs located at the NW of Kashan in Qom basin of Central Iran have been considered as candidates for the first natural gas storages in Iran. A previous 2D seismic survey across the diapir No. 4 of Shurab could not resolve the diapir structure properly and some ambiguities left unresolved. The main goal of this paper is to resolve the structure of diapir No. 4 by employing a cooperative inversion of the seismic and magnetotelluric (MT) data and a comparison with the joint inversion of transverse electric (TE) and transverse magnetic (TM) modes of the MT data. Both inversion schemes show the salt and sedimentary sequences of the stratigraphy of the Qom basin. The sequences of formations from the surface to depth are classified as upper red formation (URF), Qom formation (QF) and lower red formation (LRF). The results also show that the salt body has originated from the LRF. It is worthwhile to mention that the results from the cooperative inversion provide more details especially on the flanks and overhangs of the diapir No. 4. In addition, we have come to the conclusion that the right lateral strike-slip fault system is the most responsible phenomenon for the development of the diapirs in the survey area and the Sen–Sen fault plays a basic role as an elevator to pushing the salt up. The results are in good agreements with the resistivity and density logs of the boreholes. Moreover, the information from the geology, the cooperative inversion results on diapir No. 4, and the coincidence of the path of the Sen–Sen fault with the outcrops of the diapirs No. 1, 3 and 4 obviously provide that the tectonic scenario of the existence for diapir No. 4 could be appointed to the diapirs No. 1 and 3 equally. Another probable consequence would be the under surface continuation of the salt bodies all along the Sen–Sen fault, the verification of which requires regional MT surveys in a regular grid.

Keywords Cooperative inversion · Magnetotelluric (MT) · Seismic · Shurab diapirs · Qom basin

Introduction

Salt formations are extremely impermeable and non-reactive. The impermeability of the salt arises from the tightness of its structure and the absence of open natural joints and fissures. Moreover, flowing liquids and gases through open artificial fractures is hindered by high plastic deformability of the salt rocks. Viscoplastic deformation is an important reaction of salt against differential stresses. So this behavior closes and heals the voids and fractures just similar to the state of the ice in glaciers. In addition, a salt formation itself is not subject to changes due to the environmental events happening around it. Thus, using salt diapirs as liquid or gas storage have frequently been reported e.g. Boraiko (1985).

✉ B. Oskooi
boskooi@ut.ac.ir

[1] Institute of Geophysics, University of Tehran, Tehran, Iran

[2] Division of Geosciences and Environmental Engineering, Department of Civil, Environment and Natural Resources Engineering, Luleå University of Technology, Luleå, Sweden

[3] Department of Geophysical Methods of the Earth Crust Exploration, Moscow State University, Moscow, Russia

[4] Natural Iranian Gas Storage Company for Nasr-Abad Area, Tehran, Iran

Salt comes up through the overlying sediments in the shape of long, finger-like structures. In the area of study, in addition to the salt outcrops, the intruded salt structures exist in different depths even down to more than 3000 m (Whiting 1981). The lateral spread of the top of the salt diapirs ranges from about 750–4000 m (Chilingarian et al. 1989). Apart from the shape and dimensions, there are essential geological and geographical factors that determine whether or not a reservoir or salt cavern will make a suitable storage facility (Baikpour et al. 2016).

A salt structure in Nasr-Abad at the NW of Kashan (Fig. 1a) has been considered for the first natural gas storage project in Iran. This structure belongs to a group of diapirs so-called Shurab diapirs (SD) that have pierced the ground surface. Diapir No. 4 (the target diapir), marked by a group of hillocks, was first investigated by a 2D seismic profile (Fig. 1b). Seismic data were measured by National Iranian Oil Company (NIOC) in 1999 (ZAPCE 2016; Letouzey et al. 2006; Mokhtari 2006). The weakness of the seismic surveys to provide a clear image of the salt structure and the tectonics around diapirs are usually compensated by the magnetotelluric (MT) data. The considerable resistivity contrast between the salt bodies and surrounding sediments makes MT as an applicable tool for mapping geological and tectonic structures of the salt diapirs (Rubinat et al. 2010). The results from MT data are employed to fill the gap of geological information out of seismics by the use of either integrated interpretation or cooperative inversion schemes (Takam-Takougang et al. 2015). Thus, a high-resolution MT survey was carried out in 2013 in the Nasr-Abad area to map the subsurface resistivity distribution aiming at resolving the structure of the diapir No. 4 form Shurab diapirs. The cooperative inversion algorithm proposed by Takam-Takougang et al. (2015) and Le et al. (2016) has been implemented to improve the interpretation of the geophysical data on the diapir. The followings are the key geological questions of importance to this work. What is the source of the salt body? What is the role of the main fault of Sen–Sen regarding the

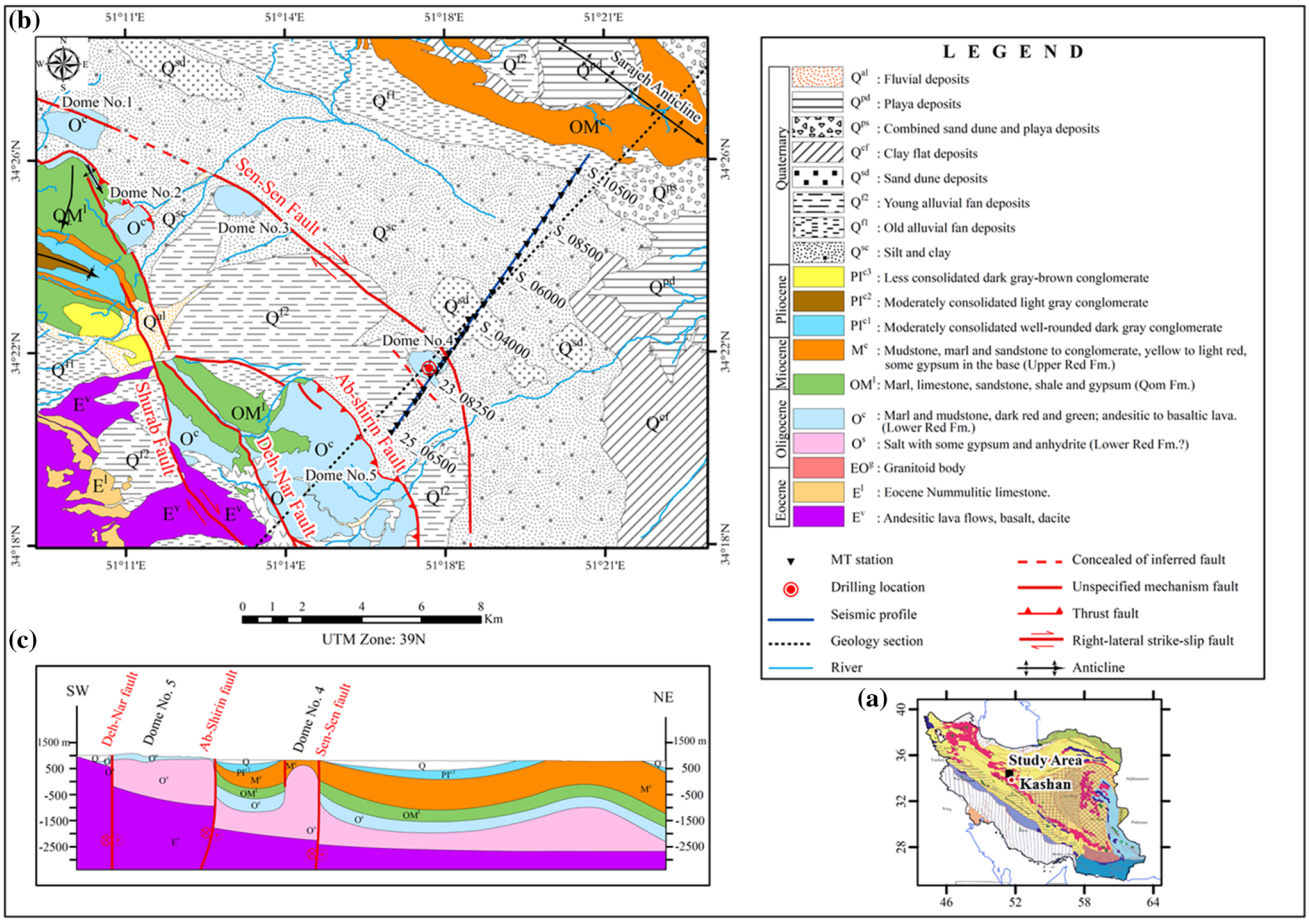

Fig. 1 **a** Location of Nasr-Abad region in the north of Kashan city on the map of important tectono-sedimentary zones of Iran (after Agha Nabati 2004) on, **b** geology map of Nasr-Abad area and **c** geological section across salt diapir No. 4 (ZAPCE 2016). Direction of displacement of Ab-Shirin and Sen–Sen faults show a dextral right lateral strike-slip fault system. Sen–Sen fault is coincident with the eastern front of diapir No. 4

uplift of the salt body? Which part of the diapir is suitable to be used as cavern? What are the reasons of piercing diapirs No. 1, 3 and 4 in the eastern side of Sen–Sen fault?

In the following sections, we introduce the geology and tectonic of the region and then continue with inversion results of the MT data and also cooperative inversion of the MT data and seismic results.

Geological setting

Central Iran (CI) is one of the most important tectonic regions in Iran due to the potential of the Qom basin and salt diapirs therein providing perfect structures of the oil reservoirs and natural gas storages (Mostofi and Gansser 1957; Abaie et al. 1963; Rosenberg 1975) so that numerous geological investigations have already been conducted in the region (Gansser 1960; Reuter et al. 2007; Jackson et al. 1990; Amini 1997). The Nasr-Abad area encompasses parts of the Urmia-Dokhtar Magmatic Arc (UDMA) and CI geological provinces in its southwestern and northeastern sectors, respectively. Therefore, it partly maintains the characteristics of both provinces of the Iran Plateau. Figure 1a shows the location of Nasr-Abad area on the map of tectono-sedimentary zones of Iran. Qom basin occupies the western part of the CI province on the northeastern side of the UDMA and is characterized by lower red formation (LRF), Qom Formation (QF) and upper red formation (URF). Figure 1b and c show the simplified geology map of the survey area and a geological section crossing the diapir No. 4, respectively.

The oldest rock units in the map area belong to the volcanic and volcaniclastic sequences of the Eocene age which is covered by LRF and mostly consists of silty shale and gypsiferous marl (Furrer and Suder 1955). Thick bodies of rock salt associated with the LRF are known to occur in embryonic salt plugs in the same area. LRF is overlaid by QF with sequences of marl, limestone, sandstone, shale and Gypsum (ZAPCE 2016). QF is covered by URF which is mostly consisting of mudstone, marl and sandstone (Stöklin and Setudehnia 1977); Gansser (1960) and Jackson et al. (1990) believe that all the salt structures of the CI region include two major salt sequences: a clean and white salt with lower Oligocene age, and a rhythmic sequence of variegated salt of upper Miocene age. These sequences are separated by QF (Abaie et al. 1963) which are not emergent in the salt structures (Talbot and Aftabi 2004).

The main tectonic evidence of the evolution of the region is known as a consequence of the collision of the Arabian and Eurasian plates in Oligocene–Miocene. The tectonic system which is probably responsible for the main development of the Shurab group of salt diapirs is probably a dextral (right-lateral) strike-slip fault system (Fig. 1b). The most important faults regarding the diapirism are Ab-Shirin and Sen–Sen faults. Ab-Shirin fault has a reverse mechanism, and should have a right-lateral strike-slip component of movement (Amini and Emami 1996). Sen–Sen is an active fault and marks the northern and eastern margins of diapirs No. 1, 3 and 4 (ZAPCE 2016). So, it is possible that the diapirs are connected in depth with Sen–Sen fault. This being the case, diapirs No. 1, 3 and 4 are piercement of salt canopy instead of scattered diapirs. Therefore, in-depth information on diapir No. 4 would shed more light on this hypothesis.

Magnetotelluric method

The magnetotelluric method was explained by Tikhonov (1950) and Cagniard (1953), and it is widely used in various applications such as oil and gas exploration (Mansoori et al. 2015), geology and tectonic (Oskooi et al. 2014, 2015), geological structures like salt diapirs (Oskooi et al. 2018), geothermal (Oskooi et al. 2005), mineral exploration (Takam-Takougang et al. 2015; Le et al. 2016), etc. Based on the assumption that the natural electromagnetic (EM) waves are plane waves, Maxwell's equations are used to extract the wave equation (Vozoff 1991; Simpson and Bahr 2005). Dependency of EM waves' attenuation to the subsurface conductivity and frequencies of the EM waves shows the diffusive nature of EM waves. So the depth that the amplitude of EM wave is reduced by e^{-1} is called skin depth, δ, and is calculated by:

$$\delta = 503\sqrt{\frac{\rho}{f}}, \tag{1}$$

where δ in meters, ρ is the resistivity in ohmm (Ωm) and f is the frequency in hertz.

From the inducing electric and magnetic fields, apparent resistivities and phases of a given frequency can be calculated through Eqs. 2 and 3:

$$\rho_a = \frac{1}{\mu_0 \omega}\left\|\frac{E}{H}\right\|^2 \tag{2}$$

and

$$\varphi = \text{phase}\left(\frac{E}{H}\right), \tag{3}$$

where, μ_0, the magnetic permeability of free space (Oskooi et al. 2014). The apparent resistivities and phases data can then be inverted to estimate geoelectrical resistivity models via inversion schemes.

MT data acquisition and processing

High-resolution MT data were acquired under the supervision of National Iranian Gas Company (NIGC) along a profile coincided with a previous seismic line (Fig. 1b). The location of MT profile (profile S) was selected in such a way to provide optimal coverage of diapir No. 4 structure in the central part of the survey area (Fig. 2). Along with this profile, 28 MT and one AMT-MT station (station 23_08250) on top of the salt body were measured. The average spacing between MT stations along profile S are 500 m except for the sites on top of the diapir No. 4 where reduced to 250 m. The azimuth of the profiles were chosen N55°E which is almost perpendicular to the main trend of regional tectonic of Sen–Sen fault. MT data were collected by the use of V5-MTU systems from the Phoenix Geophysics Ltd. The MT and AMT-MT data were measured within the period range of 0.001–1000 s and 0.0001–1000 s, respectively, for 8–12 h per each station. Also MT data were measured far away at about 10 km distance to be used for remote reference processing. The field array (magnetic sensors and electric lines) were set up according to the strike of the main tectonic boundaries considering the general strike direction of 330° which was corresponding to the *X* component, while the azimuth of 60° was corresponding to the *Y* component.

MT impedance tensor and magnetic transfer function were calculated for logarithmically spaced periods using the statistically robust method of Egbert and Booker (1986). Some examples of the result of data processing for the MT stations of S_1000, 23_08250, S_3250, S_6500 and S_08500 are shown in Fig. 3 from top to bottom, respectively. The *xy* notation defines the impedance estimated from E_x and H_y, and *yx* denotes the impedance computed from E_y and H_x. The signal period increases to the right, corresponding to the increasing depth of penetration in the Earth. Small-scale, near-surface structures can distort the electric fields and shift the apparent resistivity curves of the MT data up or down (Jones 1988; Vozoff 1991).

Physical principles governing EM distortions due to near-surface inhomogeneities have been understood for several decades and many methods have been proposed to correct the distortions. One of them is the statistical approach and it has been used for many years especially by Russian geophysicists (Berdichevsky and Dmitriev 2008). This method could be effectively used when the distance between the sites is small enough (comparable with the length of the receiving lines). The statistical correction of a static shift is based on spatial averaging of impedance along the lines. In this study, we use statistical approach to suppress the static effects on the MT data.

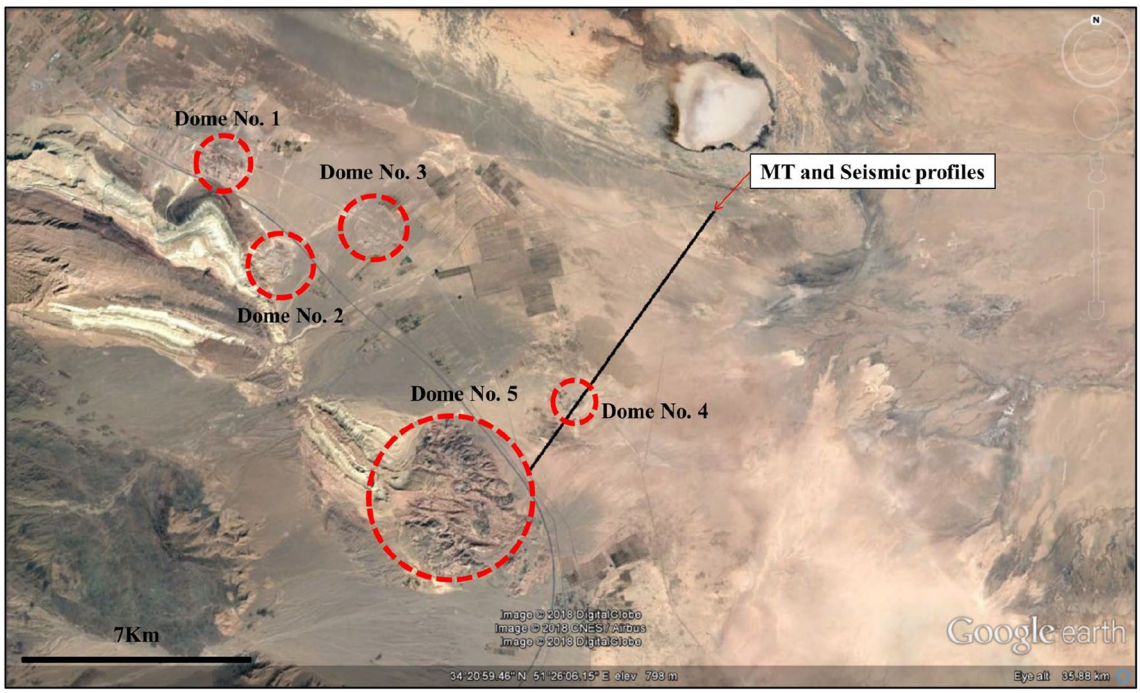

Fig. 2 Location of MT and previous 2D seismic profiles and Shurab diapirs (diapirs No. 1–5) on Google earth image (ZAPCE 2016)

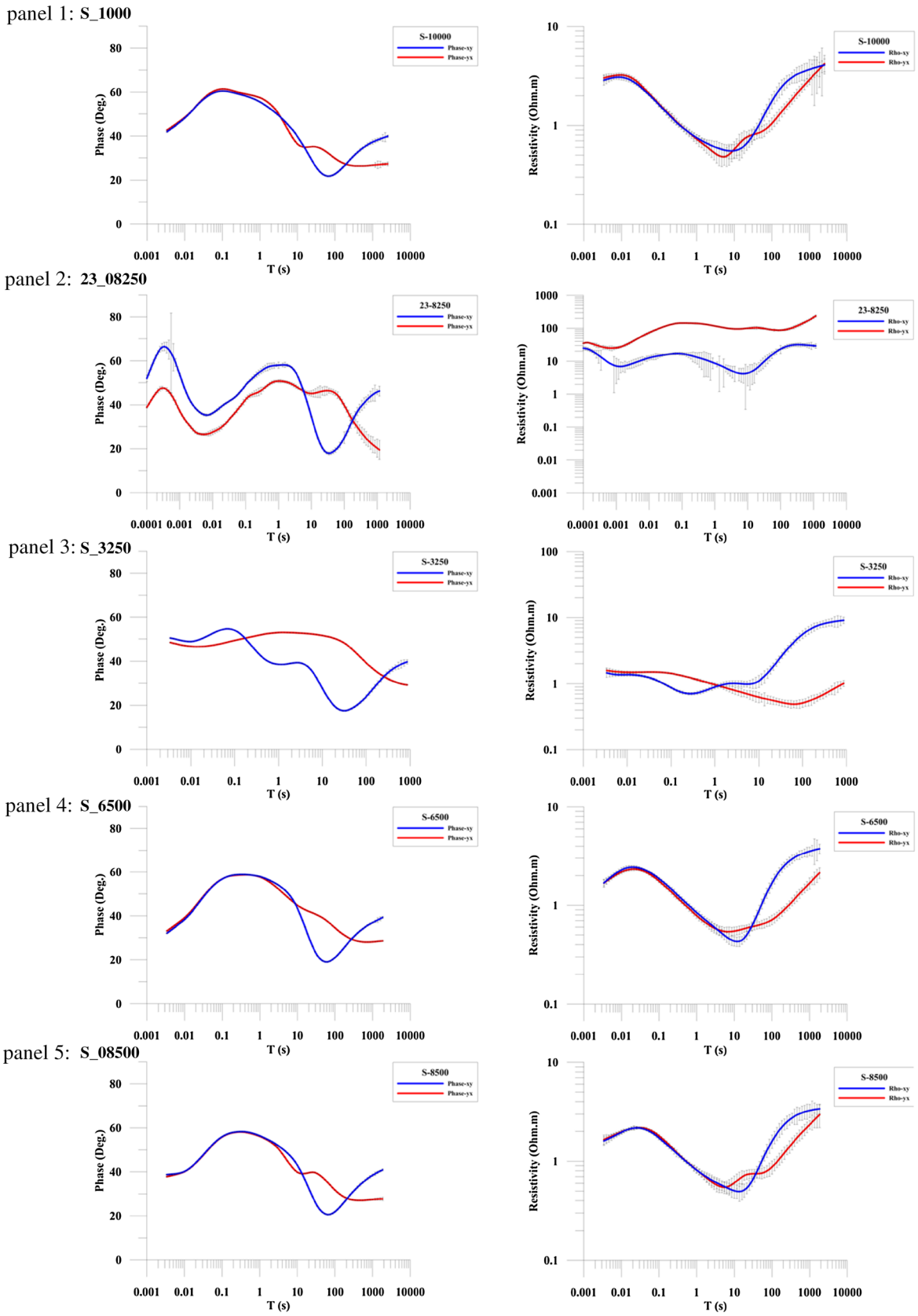

Fig. 3 Resistivity and phase curves for stations No. S_1000, 23_08250, S_3250, S_6500 and S_08500 from top to bottom, respectively. Resistivity and phase curve of station 23_08250 is distorted due to 3D condition at the top of the diapir No. 4

Dimensionality and strike analysis

The dimensionality analysis of MT data is an important stage as it helps to determine the class of interpretational model (Berdichevsky and Dmitriev 2008; Chave and Jones 2012). A number of schemes for calculating the principle components of the impedance tensor and corresponding azimuths have been proposed to determine the dimensionality and strike (e.g. Bostick 1984; Swift 1967; Vozoff 1991; Eggers 1982; Groom and Bailey 1989, 1991; Bahr 1988, 1991). The main parameters to be analyzed are inhomogeneity parameter of N, Bahr's skew (Bahr 1988, 1991), Swift's skew (Swift 1967), and β which is called phase parameter (Berdichevsky and Dmitriev 2008). These parameters have different sensitivity to different types of distortions, especially in respect to near-surface distortions, which are often called "geological noise". The inhomogeneity parameter of N and the Swift's skew behavior at long periods can be screened by near-surface features, while the phase split β and Bahr's skew are more representative.

The analysis of the inhomogeneity parameter pseudo-section confirms that the impedance tensor is 1D for the periods less than 10 s practically everywhere, except around station 23_08000 and 23_08250 where the heterogeneity starts from the period about 0.001 s. In this zone outcrop of salt diapir No. 4 is pierced on ground surface.

In Swift's skew pseudo-section, an almost 1D impedance tensor is a good approximation for period range less than 10 s except around stations 23_08000 and 23_08250 (outcrop of diapir No. 4). In this area, Swift's skew shows an anomalous part for all period range, while the phase split β anomalies are mostly localized in longer periods. Thus, we are faced with galvanic distortions between stations 23_08000 and 23_08250 corresponding to the piercing of the salt structure.

The values of the most representative Bahr's skew are low in general and only for the longer periods at the southwestern part of the profile S reach a value of 0.3. Also a little effect of 3D condition is seen in resistivity and phase curve of station 23_08250 due to measurement on the top of diapir No. 4 (Fig. 4).

The dimensionality analysis employing data from all sites and periods show a dominant 2D conductivity structure with the lowest degree of 3D distortion (Fig. 4). To proceed in matching the true geological strike, we focused our investigation on periods exceeding 10 s, since for the short periods the conductivity structure could be treated as 1D. Strike analysis around the salt outcrop slightly indicates a 3D condition. The results of the strike analyses could be supported by the surface geological observations so that taking an azimuth of 330º for the strike direction was attributed quite reasonable for applying further 2D inversion schemes.

Inversion results

By completing the dimensionality/strike analysis and static shift correction, 28 MT and one AMT-MT stations were inverted using 2D inversion approaches. The inversion strategy for this profile includes the following steps, 1D inversion of TE and TM modes, bimodal (TE + TM) 2D inversion and cooperative inversion with adding geology and seismic results.

In the first step, 1D inversion is done in TE and TM modes separately by the use of MTS-Prof Inv software from the Russian NORD-WEST Ltd. It is an automatically regularized OCCAM 1D inversion (Constable et al. 1987) for the layered half space based on Tikhonov regularization (Tikhonov et al. 1983). Results of the 1D inversion of the TM and TE modes data are shown in Fig. 5. The inversion result of TM mode (top panel in Fig. 5) shows horizontal discontinuity in the eastern and western part of diapir No. 4. While the inversion results of the TE mode (bottom panel in Fig. 5) demonstrate the deep structures more distinctly.

TE and TM modes have a potential to resolve deep and shallow structures, respectively. Because the TE and TM modes are sensitive to different features (Berdichevsky et al. 1998), 2D joint inversion of TE + TM mode data was also performed to obtain the most detailed image of the subsurface conductivity. TE mode is less sensitive to static shift effects and more robust to 3D effects caused by resistive structures (Berdichevsky et al. 1998). Therefore, low error floor is assigned for TE mode, to decrease the 3D effect and static shift effect due to the piercing of the LRF on the top of diapir No. 4. The error floors for phase and resistivity data were fixed at 2.5% and 5%, respectively, for all data modes. It is considered lower for the phase data because the phase data are less sensitive to the distortion effects than the resistivity data. To check the convergence and stability of the models, we used half-spaces with varying resistivity as initial models. We also tested different vertical and horizontal smoothing weights (Constable et al. 1987; deGroot-Hedlin and Constable 1990). Since the 1D inversion results of TE mode show a considerable correlation with the geological section, the inverted resistivity section from TE mode is selected as a starting model and equal horizontal and vertical weight was used for 2D inversion. In this step, we use both the REBOCC code of Siripunvaraporn and Egbert (2000) and the non-linear conjugate gradient (Rodi and Mackie 2001) algorithm included in the MT2DTools. The results of the 2D bimodal inversion resolve the location of the salt diapir properly (Fig. 6). Also conductive members of URF and LRF are separated by the resistive part of QF. Comparison of the results from 2D inversion with geological information shows that the eastern boundary of the diapir No. 4 is not completely delineated in the resistivity model.

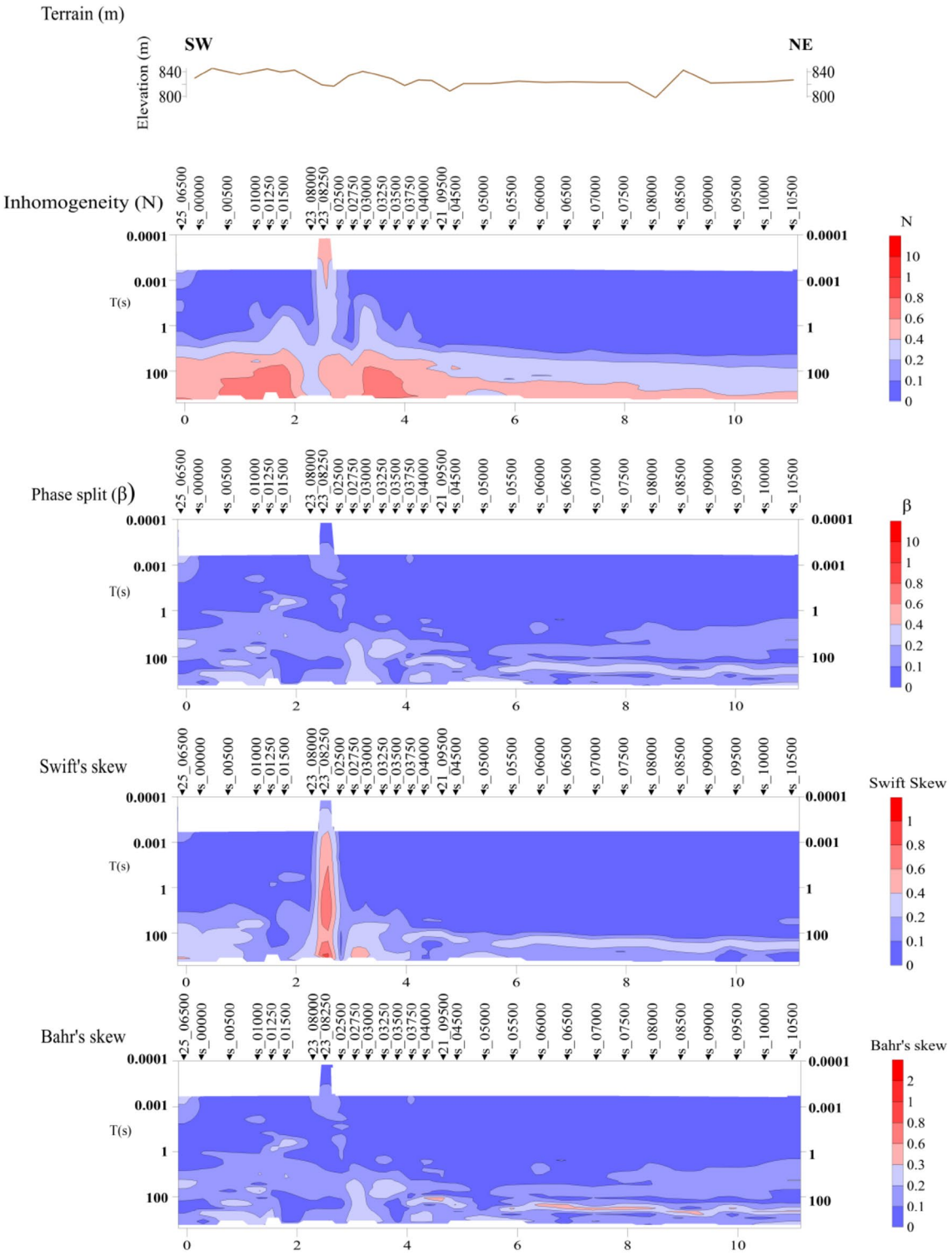

Fig. 4 Dimensionality analysis, surface topography, amplitude inhomogeneity parameter (N), phase split (β), Swift's skew and Bahr's skew from top to bottom. Inhomogeneity parameter shows the presence of 2D structure on diapir No. 4 and it is verified by Swift's skew as well. Results of Bahr's skew show no notable distortions due to the 3D effect

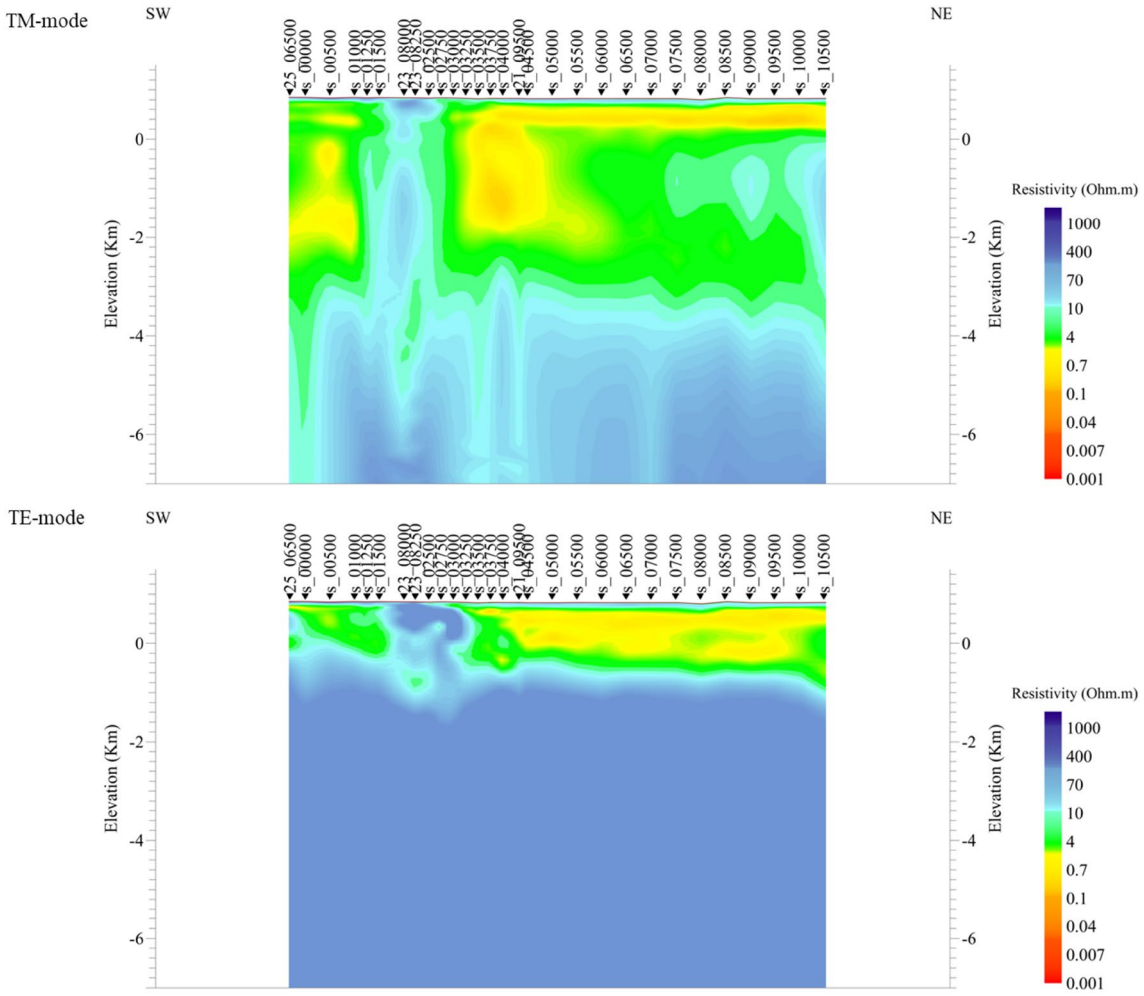

Fig. 5 1D inversion results of TM and TE mode data. Resistivity model of the TM mode data shows the boundaries of the diapir No. 4 more accurately than the model of the TE mode data. But the TE mode data resolves the resistivity values more properly than the TM mode data, especially at the location that diapir No. 4 is pierced

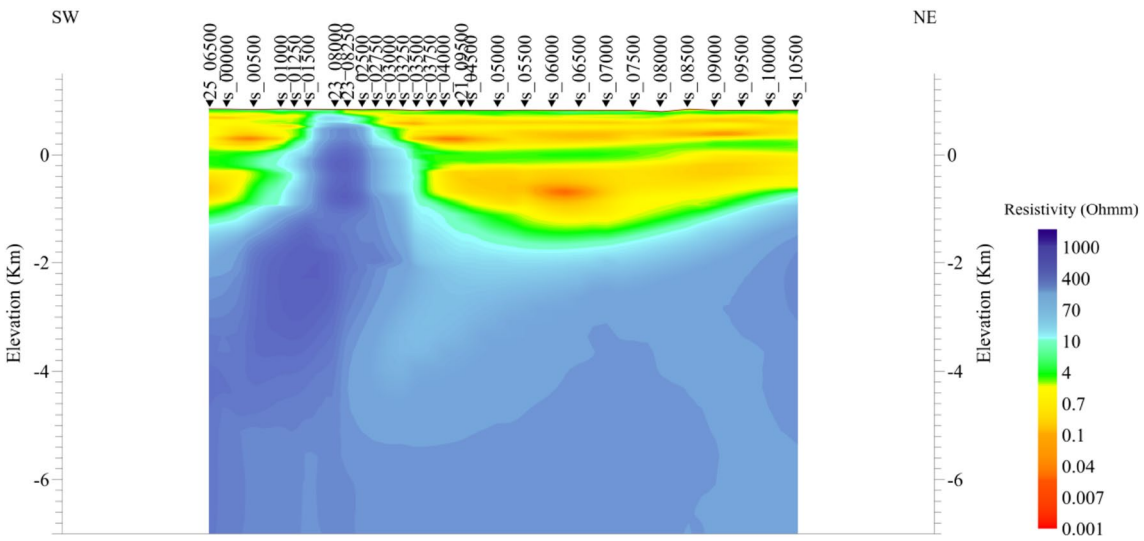

Fig. 6 The resistivity model out of the 2D inversion of the MT data along profile S

To improve the inversion of the MT data in the cooperative inversion scheme, the seismic horizons and the locations of the faults were added as constraints while running the REBOCC code. Geological information and seismic horizons are added by the use of Le et al. (2016) approach. Then to achieve a lower root mean square (RMS) error, the final results of the constraint inversion in REBOCC were used as the starting model for the MT2DTools software. In this step, we decrease the value of the Lagrange multiplier to resolve the model parameters in more details (Fig. 7).

The convergence to a possible minimum RMS misfit was achieved after about 150 iterations for all stages in 2D inversion. The data misfits for almost all the data-modes were generally satisfactory indicating that the observed data are well-fitted to the forward responses. TM mode is more sensitive to 3D effect and also to the static shifts resulted from the resistive bodies. So, the more weight in inversion (equal to lower error floor) is put on TE mode. As a result of this inversion strategy, a neglecting mismatch is seen in period range 0.01–100 s and stations s_01000–s_03250 of TM

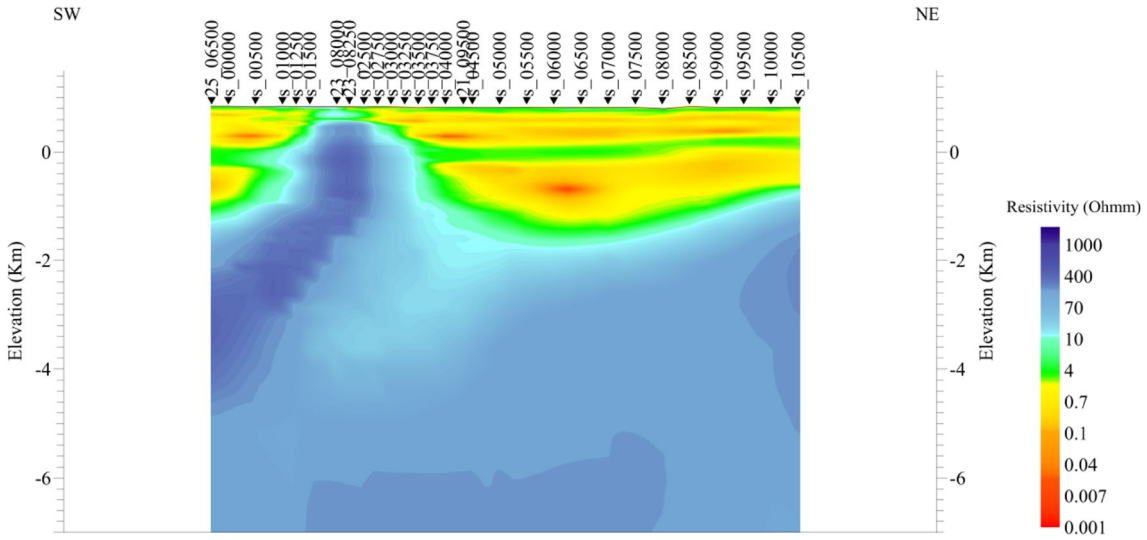

Fig. 7 The resistivity model out of cooperative inversion of the MT data along the profile S

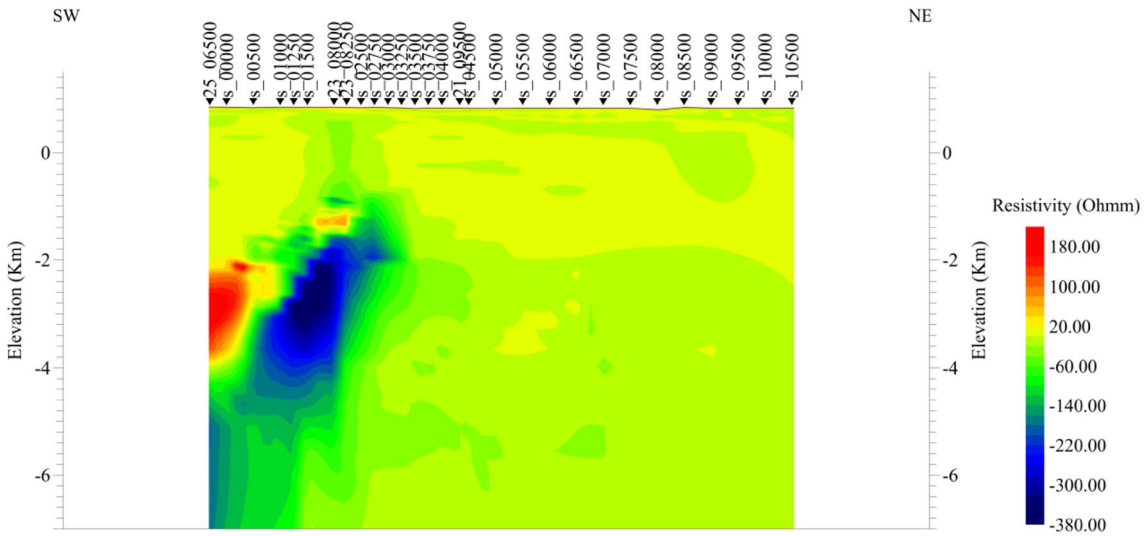

Fig. 8 Difference between the resistivity section from the 2D bimodal inversion and the cooperative inversion results depicted in Figs. 6, 7, respectively. The red color shows that the resistivity in the cooperative inversion is increased while the blue is related to the decrease in the resistivity value. It should be noted that the results of the cooperative inversion delineate the salt body in depth. In addition, cooperative inversion results increase the resolution of resistivity model in the shallow part of diapir but reflects minor responses in the sedimentary sequence at the rest of the section

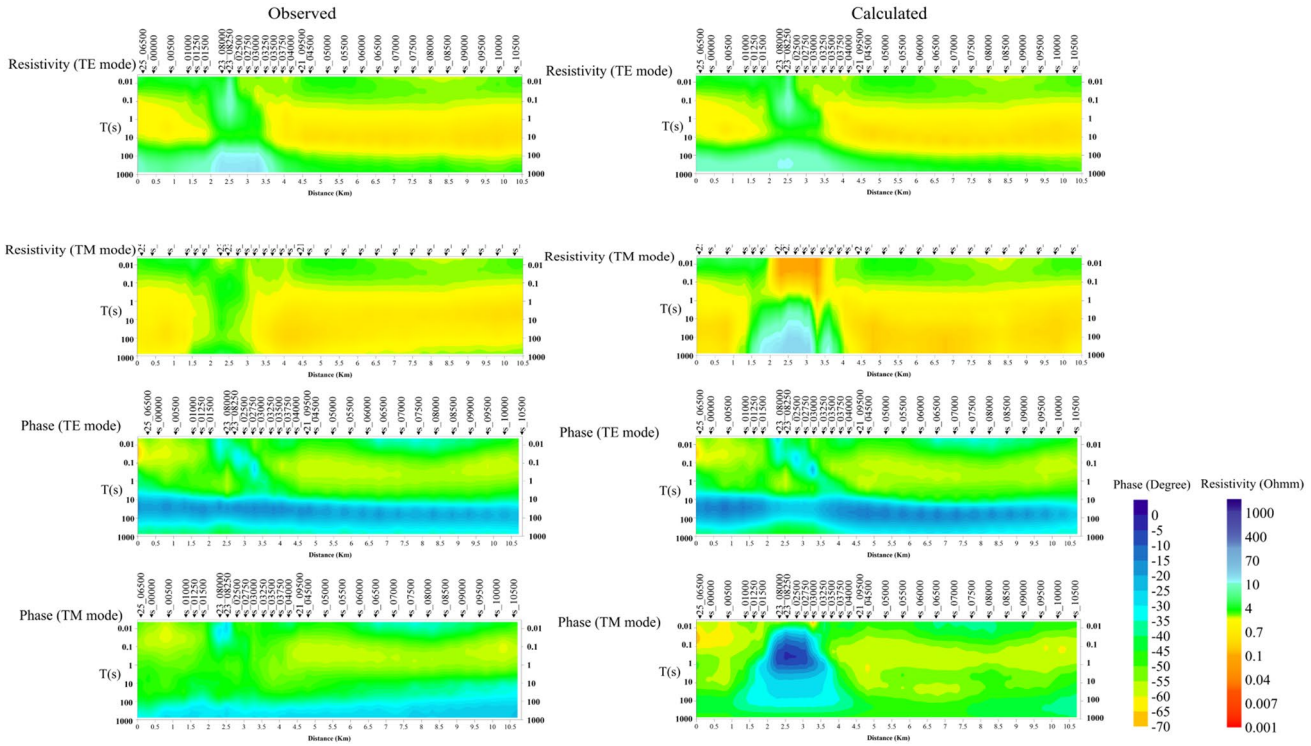

Fig. 9 Observed MT data as the apparent resistivities and phases along profile S and corresponding model responses are shown

mode (Fig. 9). Cooperative inversion method along this profile resolves a finger like shape of salt body and the eastern and western boundaries of the diapir No. 4. more clearly. To show the difference between these results, the numeric difference in resistivity values of the model parameters between the two inversion models is shown in Fig. 8. The Difference between the two resistivity values of the cooperative and the 2D bimodal inversion is large in the western part of the MT profile at the depth range of about 2–6 km.

Interpretation and discussion

Previous seismic results on diapir No. 4 were of poor quality-especially at its overhangs and flanks-due to the complex geological structure of the diapir. The complexity of the geological structure arises from the exposure of heterogeneous gypsiferous sediments and dissolution cavities from the surface to the depth of about 200 m. However, MT data can produce complementary information due to the resistivity contrast of the salt and surrounding sediments. On the other hand, diffusive nature of the electromagnetic waves provides a smooth image of the salt body. It should be noted that in most cases, sedimentary layers in a basin can clearly be resolved by seismic data. Therefore, in our case, a cooperative inversion scheme is used to integrate any valuable information from seismic data to the inversion process of the MT data. In the following, first the results out of the 2D bimodal inversion of the MT data are interpreted, then the cooperative inversion of seismic and MT data is discussed.

2D resistivity models derived from the joint inversion of the TE- and TM-mode data show the sequences of the geological stratigraphy properly. From the surface down to the deep structures, a conductive (5–10 Ωm) near surface layer corresponding to the fine quaternary sediments saturated with brackish water, a more conductive (less than 5 Ωm) underlying layer correlated with the URF and marly part of QF are resolved, respectively. Deeper down the resistivity is increasing up to 20 Ωm due to the limestones and sandstones of the QF. Then the resistivity is decreasing to less than 1 Ωm which is related to the shale and gypsum of the QF as well as the marl and mudstone of the LFR. The very resistive half space (more than 4000 Ωm) at the deepest part of the section is attributed to the andesitic to basaltic lavas, the salt with gypsum and anhydrite of the LRF and the volcanic rocks of Eocene.

Comparing the 2D bimodal inversion and the cooperative inversion sections show that from the results of the cooperative inversion we can distinguish the western and eastern boundaries of the salt and simultaneously the general shape of the salt body. In the resistivity sections of Figs. 6 and 7, we can see the conductive anomalies in the western and eastern sides of the diapir at the elevation of about 400 m down to the depth of 1600 m. Those parts consist of

the sequentially layered sediments which show the lowest changes (see Fig. 8) when applying the two different inversion schemes. Flow of surface water and groundwater on the top of or into the gypsiferous and salty media cause aggregation of dissolution ions in groundwater (Nekouei et al. 2016). These zones are resolved as the conductive anomalies in both sides of the diapir. It should be noted that cooperative inversion can delineate the diapir geometry more accurately in agreement with the geological information while the 2D bimodal inversion provides a smooth image of the model in depth. Also, cooperative inversion clearly shows that the eastern front of the diapir is limited to the Sen–Sen fault.

In the following, we focus on the interpretation of the cooperative inversion model only. As could be seen in Figs. 10 and 11, the resistivity discontinuity in the eastern part of the salt body coincides with the surface track of the Sen–Sen fault. Integrated interpretation of the resistivity and geology shows that Sen–Sen fault plays the role of uplifting the salt. Location and the effects of this fault are not resolved by seismics (Figs. 10 and 11). Comparison between a strike-slip fault system (Fig. 1b) and up-coming pattern of a salt body verifies the role of the dextral (right-lateral) strike-slip fault system which can be extended to the especial situation of the Sen–Sen fault.

The resistivity and density logs and geological information from drilling location (Fig. 1b) from the depth of 400–900 m are compared with cooperative inversion results (Fig. 10). Resistivity values in MT section is exceeded to more than 4000 Ωm for the salt formation due to the existence of cavities in the upper part of the diapir. It is also obvious that the sharp variation in the resistivity and density logs is due to the existence of those cavities (Fig. 10). As could be seen in the resistivity log, the highest resistivity value is related to the salt body. Although thin layers of andesite and claystone (less than 50 m) with lower resistivities are reported in the resistivity log, they are not seen in the section due to their small thicknesses. The density log shows variations through andesite and claystone layers but it shows the lowest values through the salt body.

To compare all information including geology, resistivity and post-stack depth migration (PSDM) section of the seismic data, the 3D view of Fig. 11 is prepared. An evaluation on the displacement directions of the Ab-Shirin and Sen–Sen faults (two right-lateral strike-slip faults) and

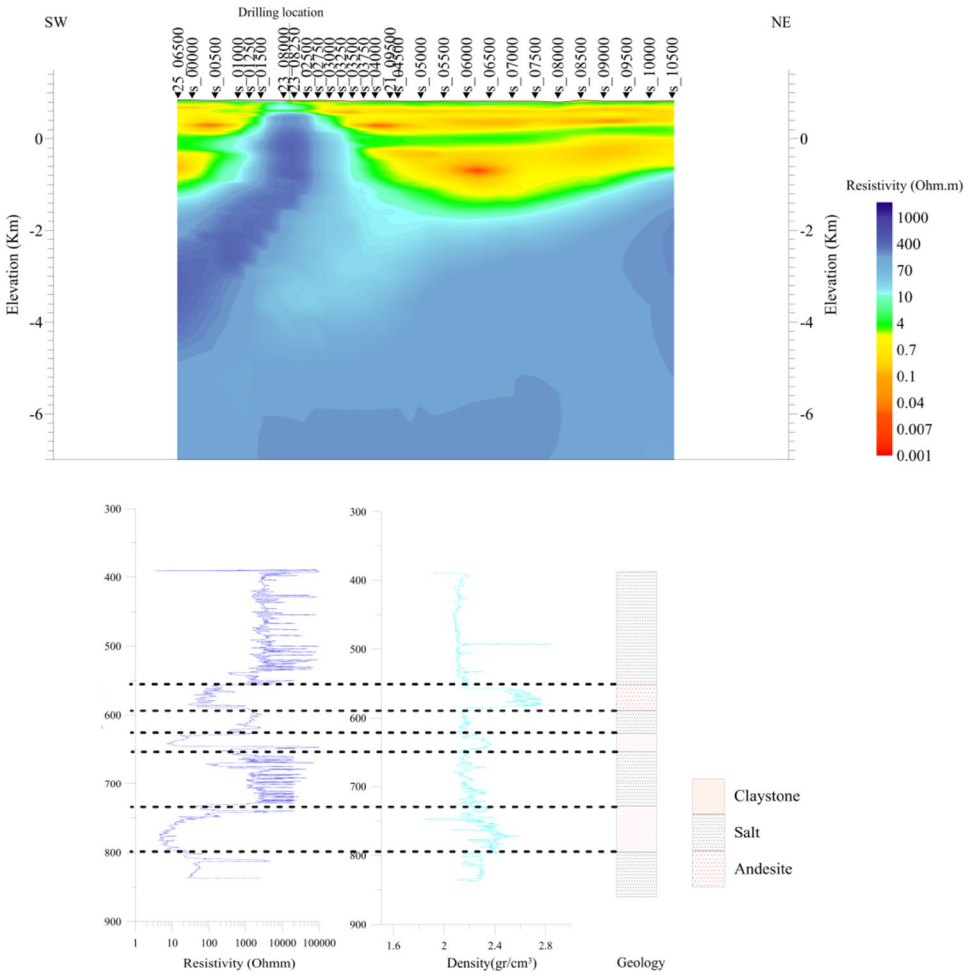

Fig. 10 Inversion result from cooperative inversion (top panel) and resistivity and density log and geology information from drilling (lower panel). Notice that the variations of the resistivities and densities coincide with the changes in the geological stratigraphy, i.e., for example, the salt layers in the well log are presented with the highest values in resistivity and lowest values in density

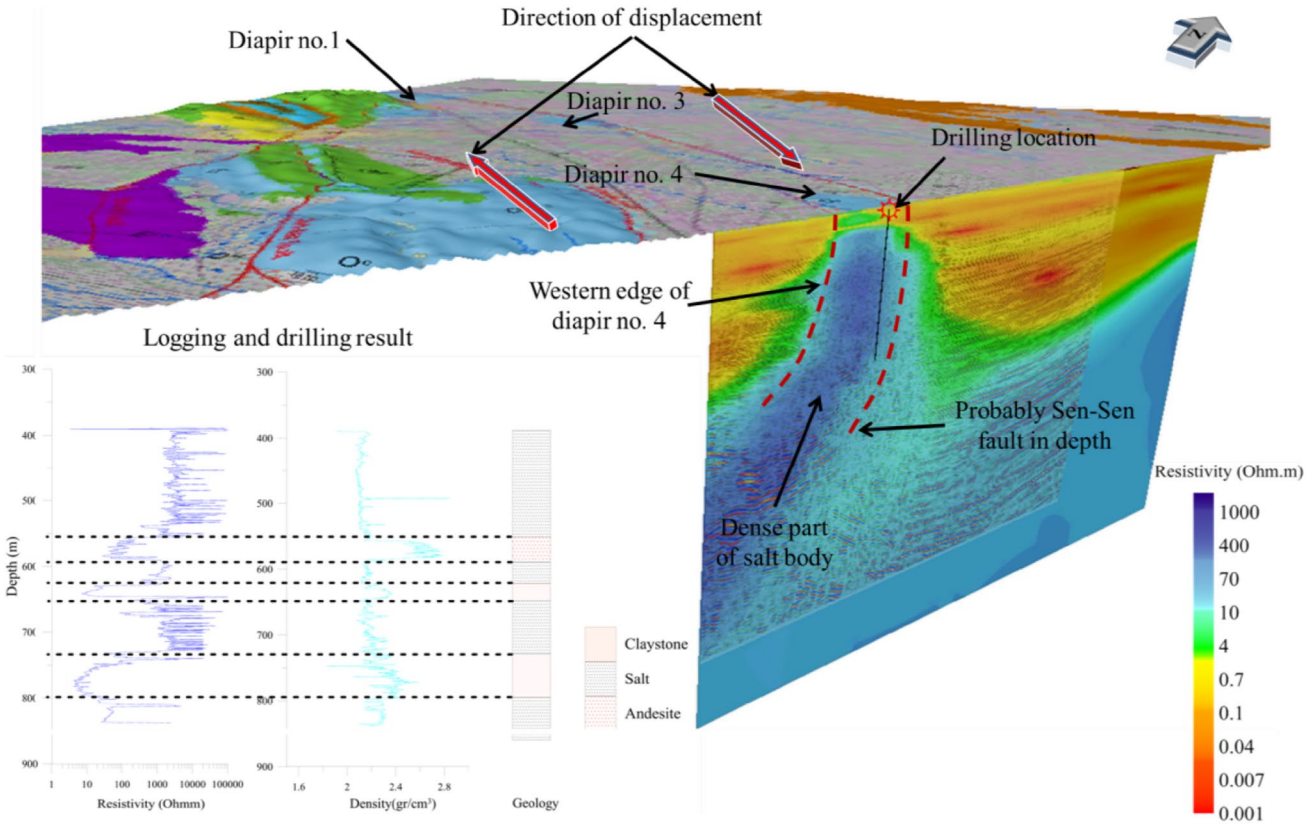

Fig. 11 Comparison between geology, seismic and resistivity and density logs across diapir No. 4. Mention that the eastern boundary of diapir No. 4 is resolved more precisely in the results of the cooperative inversion and coincides with the surface track of Sen–Sen fault (As could be seen in Fig. 8, the cooperative inversion results provide more details of diapir structures, especially in depth.). Being the case, the track of Sen–Sen fault is drawn in depth based on the resistivity model of cooperative inversion. In addition, it should be noted that the direction of displacement of Sen–Sen and Ab-Shirin faults and the shape of salt diapir verify the role of the dextral (right-lateral) strike slip fault system in uplifting the salt. It should be considered that the effect of Sen–Sen fault is not resolved in the seismic section while the good reflection from sedimentary horizons are coincident with the resistivity section

considering the effects of those faults causing the outcrops of salt diapirs in the survey area (at the locations of diapirs No. 1, 3 and 4 show that the tectonic scenario for diapir No. 4 can be extended to diapirs No. 1 and 3. In addition, results from dimensionality analysis (Fig. 4) show the 2D behavior of diapir No. 4. Again it is confirmed that the salt body in depth is probably continuous along Sen–Sen fault. So it is expected that we encounter a salt wall (salt canopy) instead of dispersed diapirs (diapirs No. 1, 3 and 4).

Conclusion

Salt diapirs are used as liquid or gas storage because salt formations are extremely impermeable and non-reactive geological structures. Diapir No. 4 from Shurab diapirs located at the NW of Kashan is selected as the first natural gas storage in Iran. It was initially investigated using a 2D seismic survey (ZAPCE 2016). Seismic results were of poor quality at the overhangs and flanks of the diapir (Letouzey et al. 2006) while the MT data could provide considerably good results due to the sharp resistivity contrast between salt body and surrounding sediments. So, 28 MT and 1 AMT stations are measured along a profile coinciding with the previous seismic profile. Apart from 2D bimodal inversion, geophysical model is improved by adding seismic information with cooperative inversion of the MT and seismic methods. Although the seismic survey could not depict diapir structure properly, it could be used to justify the results of 2D bimodal inversion and cooperative inversion of seismic and MT methods and minimize the ambiguities associated with the interpretation of the diapir structure as well.

The results of the 2D bimodal inversion are compared with cooperative inversion results as well. The results from the 2D bimodal inversion show the finger shape of the salt diapirs and the sedimentary sequences of the Qom basin's stratigraphy. In addition, it is confirmed that the origin of the salt body is from the LRF and there is no evidence of the conductive URF (in comparison with resistive salt body) and QF. On the other hand, the results out of the 2D bimodal

inversion could not delineate the eastern front of the diapir and the location of the Sen–Sen fault precisely due to the diffusive nature of electromagnetic waves. However, the results from the cooperative inversion of the seismic and MT data show not only the finger shape of the salt diapir more properly but also the effect of Sen–Sen fault as the eastern limit of the diapir No. 4 is delineated completely. Also the up-coming pattern of the salt body verifies the role of the dextral (right-lateral) strike slip fault system of the Sen–Sen and Ab-Shirin faults.

A comparison between the resistivity values from the inversion with the resistivity and density logs and the geological information from drilling shows a good agreement. So it seems that the best location and depth for producing cavern in the pure salt could be found based on the resistivity value. Comparing the direction of displacement of the Ab-Shirin and Sen–Sen faults (two right-lateral strike-slip faults) shows that the strike of the Sen–Sen fault coincide with the outcrops of the salt diapirs No. 1, 3 and 4. This shows that the tectonic scenario for diapir No. 4 could also be matched with the diapirs No. 1 and 3 as well. In addition, the dimensionality analysis of MT data in the vicinity of diapir No. 4, shows the presence of a 2D structure in the region. So, it is probable that salt body is continuous along the Sen–Sen fault. Based on this hypothesis, one can expect the existence of a salt canopy along the Sen–Sen fault instead of dispersed diapirs. We suggest conducting a regional MT survey to identify the subsurface connection between the diapirs indeed.

Acknowledgements This work was originally funded by the research council of the University of Tehran (UT) in Iran. The second author acknowledges funding from the UT under the mission commandment No: 155/96/1894 dated 2017/12/23 for a 1-year sabbatical leave starting from 2018/01/21 at the Luleå University of Technology in Sweden. We thank the National Iranian Gas Storage Company for supplying the geophysical data which were collected by the Russian North West company. We are also grateful to the Zamin Ab Pey Company for supplying the hardware and software, as well as logistical support when we prepared and analysed the data. We are thankful to M. J. Bolourchi for consulting us in geology and tectonic of Nasr-Abad area. The NORDWEST group is also acknowledged for scientific advice.

References

Abaie IL, Ansari HJ, Badakhshan A, Jafari A (1963) History and development of the Alborz and Serajh fields, central Iran. In: Proceedings of the 6th world petroleum conference, Frankfurt, section 2, pp 000–111

Agha Nabati A (2004) Iran's geology. Geological survey of Iran, Tehran, Iran

Amini A (1997) Provenance and depositional environment of the upper red formation, central zone, Iran. Doctoral dissertation, Manchester University

Amini B, Emami MH (1996) Geological map of Aran, scale 1:100,000. Geological survey of Iran, Tehran, Iran

Bahr K (1988) Interpretation of the magnetotelluric impedance tensor: regional induction and local telluric distortion. Geophysics 62(2):119–127

Bahr K (1991) Geological noise in magnetotelluric data a classification of distortion types. Phys Earth Planet Inter 66(1–2):24–38

Baikpour S, Motiei H, Najafzadeh K (2016) Geological and geophysical study of salt diapirs for hazardous waste disposal. Int J Environ Sci Technol 13(8):1951–1972

Berdichevsky MN, Dmitriev VI (2008) Models and methods of magnetotellurics. Springer Science & Business Media, Germany

Berdichevsky MN, Dmitriev VI, Pozdnjakova EE (1998) On two-dimensional interpretation of magnetotelluric soundings. Geophys J Int 133(3):585–606

Boraiko AA (1985) Storing up trouble hazardous waste. Natl Geogr Mag 167(3):318–351

Bostick FX (1984) Electromagnetic array profiling survey method. U.S. Patent No. 4, Washington, DC: U.S. Patent and Trademark Office, pp 591–791

Cagniard L (1953) Basic theory of the magneto-telluric method of geophysical prospecting. Geophysics 18(3):605–635

Chave AD, Jones AG (2012) The magnetotelluric method, theory and practice. University Press, Cambridge

Chilingarian GV, Robertson JO, Kumar S (1989) Surface operations in petroleum production. Elsevier, USA, II

Constable SC, Parker RL, Constable CG (1987) Occam's inversion: a practical algorithm for generating smooth models from electromagnetic sounding data. Geophysics 52(3):289–300

deGroot-Hedlin C, Constable CG (1990) Occam's inversion to generate smooth, two-dimensional models from magnetotelluric data. Geophysics 55(12):1613–1624

Egbert GD, Booker JR (1986) Robust estimation of geomagnetic transfer functions. Geophys J R Astron Soc 87(1):173–194

Eggers DE (1982) An eigenstate formulation of the magnetotelluric impedance tensor. Geophysics 47(8):1204–1214

Furrer MA, Suder PA (1955). The Oligo–Miocene marine formation in the Qom region (Iran). In: 4th World Petroleum Congress. World Petroleum Congress, 1–1

Gansser A (1960) Die geologische erforschung der Qom gegend. Iran. Bull Ver Schweitzerisches Pet-Geol Ing 23:1–16

Groom RW, Bailey RC (1989) Decomposition of magnetotelluric impedance tensor in the presence of local three-dimensional galvanic distortion. J Geophys Res Solid Earth 94(B2):1913–1925

Groom RW, Bailey RC (1991) Analytic investigations of the effects of near-surface three-dimensional galvanic scatters on MT tensor decompositions. Geophysics 56(4):496–518

Jackson MPA, Cornelius RR, Craig CH, Gansser A, Stöklin J, Talbot CJ (1990) Salt diapirs of the great Kavir, Central Iran. Geol Soc Am Mem 177:139

Jones A (1988) Static shift of MT data and its removal in a sedimentary basin environment. Geophysics 53(7):967–978

Le CVA, Harris BD, Pethick AM, Takam-Takougang EM, Howe B (2016) Semiautomatic and automatic cooperative inversion of seismic and magnetotelluric data. Surv Geophys 37(5):845–896

Letouzey J, Baghbani D, Rudkiewicz JL, Cuilhe L, Kazemi K (2006) Structural evolution and hydrocarbon accumulation in Central Iran, Qum region. In: 68th EAGE conference and exhibition incorporating SPE EUROPEC

Mansoori I, Oskooi B, Pedersen LB (2015) Magnetotelluric signature of anticlines in Iran's sehqanat oil field. TectonoGeophysics 654:101–112

Mokhtari M (2006) Application of seismic and well data in determination of porosity in Serajeh Gas Field. Master thesis of Geophysics, University of Tehran **(in Persian)**

Mostofi R, Gansser A (1957) The story behind the 5 Alborz. Oil Gas J 55:78–84

Nekouei E, Zarei M, Raeisi E (2016) The influence of diapir brine on groundwater quality of surrounding aquifers, Larestan. Iran. Environ Earth Sci 75(7):571

Oskooi B, Pedersen LB, Smirnov M, Arnasson K, Esteinsson H, Manzella A, the DGP working group (2005) The deep geothermal structure of the Mid-Atlantic ridge deduced from MT data in SW Iceland. Phys Earth Planet Inter 150(1–3):183–195

Oskooi B, Pedersen LB, Koyi HA (2014) Magnetotelluric signature for the zagros collision. Geophys J Int 196(3):1299–1310

Oskooi B, Mansoori I, Pedersen LB, Koyi HA (2015) A magnetotelluric survey of ophiolites in the Neyriz area of southwestern of Iran. Pure Appl Geophys 172(2):491–502

Oskooi B, Moradi M, Pushkarev P (2018) Magnetotelluric study on a diapir in Qom basin, central Iran. In: 24th EM Induction Workshop, Helsingør

Reuter M, Piller WE, Harzhauser M, Mandic O, Berning B, Rogl F, Kroh A, Aubry MP, Wielandt-Schuster U, Hamedani A (2007) The Oligo–Miocene Qom formation (Iran): evidence for an early Burdigalian restriction of the Tethyan seaway and closure of its Iranian gateways. Int J Earth Sci 98(3):627–650

Rodi WL, Mackie RL (2001) Nonlinear conjugate gradients algorithm for 2D magnetotelluric inversion. Geophysics 66(1):174–187

Rosenberg R (1975) Qum-1956: a misadventure in Iranian oil. Bus Hist Rev 49(1):81–104

Rubinat M, Ledo J, Roca E, Rossel O, Queralt P (2010) Magnetotelluric characterization of a salt diapir: a case study on Bicorb-Quesa diapir (Prebetic Zone, SE Spain). J Geol Soc 167(1):145–153

Simpson F, Bahr K (2005) Practical magnetotellurics. University Press, Cambridge

Siripunvaraporn W, Egbert G (2000) An efficient data-subspace inversion method for 2-D magnetotelluric data. Geophysics 65(3):791–803

Stöklin J (1977) Stratigraphic lexicon of Iran. Geol Surv Iran 18:376

Swift CM (1967) A magnetotelluric investigation of an electrical conductivity anomaly in the southwestern United States. Doctoral dissertation, Massachusetts Institute of Technology

Takam-Takougang EM, Harris B, Kepic A, Le CVA (2015) Cooperative joint inversion of 3D seismic and magnetotelluric data: with application in a mineral province. Geophysics 80(4):R175–R187

Talbot CJ, Aftabi P (2004) Geology and models of salt extrusion at Qom Kuh, Central Iran. J Geol Soc 161(2):321–334

Tikhonov AN (1950) The determination of electrical properties of deep layers of the earth's crust. Dokl Acad Nauk SSR 73:295–297

Tikhonov AN, Goncharsky AV, Stepanov VV, Yagola AG (1983) Regularizing algorithms and a priori information. Mir, Moscow

Vozoff K (1991) The magnetotelluric method. In: electromagnetic methods in applied geophysics-application Parts A and B. Soc Explor Geophys 2:641–712

Whiting GH (1981) Strategic petroleum reserve (SPR) geological site characterization report, Sulphur Mines Salt Domes. In: SAND80-7141, Sandia National Labratories, Allbuquerque, NM

ZAPCE (2016) Geological evaluation and seismicity on the salt structure of Nasrabad Kashan. Report no. 1 to the Natural Gas Storage Company of Iran